
Anisotropy of acoustooptic figure of merit for TeO₂ crystals.

2. Anisotropic diffraction

Mys O., Kostyrko M., Krupych O. and Vlokh R.

Vlokh Institute of Physical Optics, 23 Dragomanov Street, 79005 Lviv, Ukraine,
vlokh@ifo.lviv.ua

Received: 02.02.2015

Abstract. We present the developed method for analyzing the anisotropy of acoustooptic figure of merit (AOFM) for the case of anisotropic diffraction in optically uniaxial crystals, and we illustrate it on the example of crystalline paratellurite. We demonstrate that nine types of acoustooptic (AO) interactions can be implemented in general, six types for the isotropic interactions and three for the anisotropic ones. When the AO diffraction is collinear, the angular dependence of the AOFM is characterized by narrow peaks or dips. In the case of anisotropic diffraction, the maximum AOFMs for the paratellurite crystals are reached for the AO interactions of the type VIII with the acoustic wave QT₁ propagated along the [110] direction and are polarized along [̄10]. The AOFM is equal to $929 \times 10^{-15} \text{ s}^3/\text{kg}$ in this case. Nonetheless, the highest AOFM value for TeO₂ crystals ($1143.8 \times 10^{-15} \text{ s}^3/\text{kg}$) can be reached when linearly polarized optical eigenwaves interact isotropically with the transverse acoustic wave QT₁ (see *Mys O. et al, 2014. Ukr. J. Phys. Opt. 15: 132*). This AO diffraction belongs to the type III. The results of our calculations agree well with the experimental data known from the literature.

Keywords: acoustooptic figure of merit, effective elastooptic coefficients, paratellurite crystals, anisotropy

PACS: 43.35.Sx, 42.70.Mp

UDC: 535.012.2+535.42+534.321.9

1. Introduction

In the first part of the present study [1] we have considered spatial anisotropy of acoustooptic figure of merit (AOFM) for TeO₂ crystals under the conditions of isotropic acoustooptic (AO) interactions. Six different types of isotropic interactions have been analyzed in this work. We have found that the highest AOFM value, $M_2^{(III)} = 1143.8 \times 10^{-15} \text{ s}^3/\text{kg}$, is reached when we deal with the type III of AO interactions. Then the incident optical wave which is polarized almost parallel to the direction [001] and propagates in the principal plane XY (i.e., in the crystallographic plane ab) interacts with the quasi-transverse acoustic wave (AW) QT₁. The latter propagates in the same plane ab almost parallel to the [110] direction, being polarized along [̄110]. We have concluded that the high M_2 value mentioned above represents a combined result of a high effective elastooptic coefficient (EOC) and a notable slowness of the AW.

Since TeO₂ is an optically uniaxial crystal with a large natural birefringence, anisotropic types of AO interactions can also be implemented in this material. For example, it is known that the anisotropic AO interactions yield in the AOFM equal to $1200 \times 10^{-15} \text{ s}^3/\text{kg}$ for the circularly polarized incident wave [2] and to 600×10^{-15} – $800 \times 10^{-15} \text{ s}^3/\text{kg}$ for the linearly polarized incident

wave [2, 3]. Thus, the anisotropic AO diffraction can also be highly efficient in different crystals, in particular in the paratellurite. Moreover, this type of diffraction has some additional importance since it is accompanied by a switching of light polarization. To our best knowledge, the methods suitable for analysing AOFM anisotropy for the anisotropic AO diffraction have not yet been developed. In fact, we know only one work [4] where angular dependence of the effective EOC has been calculated for LiNbO₃ crystals at the collinear geometry of AO interactions. As a consequence, in the present part of our AO studies we plan to develop a method for analyzing the AOFM anisotropy for the anisotropic type of AO diffraction in crystals, using the case of crystalline tellurium dioxide as a suitable example.

2. Methods of analysis

To analyze the AOFM anisotropy at the isotropic diffraction, earlier we have developed the methods for analyzing the anisotropy of EOC and AW slowness [1]. Derivation of the EOC assumes searching for an EOC responsible for the refractive index change for the incident and diffracted light waves, which have the same polarization at the isotropic diffraction. In case of the anisotropic diffraction, the polarizations of the incident and diffracted waves differ. Then the analysis should follow from the condition of difference from zero of a relevant coupling coefficient κ . One can employ the coupled mode equations:

$$\frac{\partial A_1}{\partial x} = -\kappa A_2, \quad \frac{\partial A_2}{\partial x} = -\kappa^* A_1, \quad (1)$$

where A_1 and A_2 are the amplitudes of the coupled waves, and the asterisk indicates complex conjugating. The coupling coefficient is given by the relation [5]

$$\kappa = \frac{\omega}{4n_i c \cos \theta_B} \left| p_1^* n_i^2 (\text{pe}) n_d^2 p_2 \right|, \quad (2)$$

where ω is the light frequency, θ_B the Bragg angle, p_1, p_2 are the unit polarization vectors respectively for the incident and diffracted light waves, n_i denotes the refractive index of the incident wave propagating at the Bragg angle, n_d the refractive index for the diffracted wave, c the light speed in vacuum, and (pe) the matrix with the components $p_{ij} e_j$ (with p_{ij} and e_j being the elastooptic (EO) tensor and the strain tensor, respectively). In the case of anisotropic diffraction, p_1 and p_2 differ and the EO tensor p_{ij} written in the eigen-coordinate system of the Fresnel ellipsoid should contain nonzero components p_{4j}, p_{5j} and p_{6j} . However, the latter holds true for the interactions taking place in the principal crystallographic planes only, while different EOCs can participate in the interaction in the contrary cases. As a result, one has to consider three types of anisotropic AO interactions in crystals. They are concerned with longitudinal (a type VII) and transverse (types VIII and IX) AWs.

Let us consider the AO interaction in ZX plane of optically positive paratellurite crystals belonging to the tetragonal point symmetry group 422 [6]. Their refractive indices are equal to $n_o = 2.2597$ and $n_e = 2.4119$ at the light wavelength of $\lambda = 632.8$ nm [7]. As mentioned in the study [1], the results of our analysis should also apply to the crystals of the symmetry groups 4/mmm, 422, $\bar{4}2m$ and 4mm, since the fourth-rank tensors of EOCs and elastic stiffness coefficients are the same for all the groups mentioned.

Let the incident optical wave propagate at the angle θ with respect to the X axis and let the diffracted wave propagate at the angle γ with respect to the wave vector of the incident light wave

(see Fig. 1). Here the incident wave is assumed to be polarized as ordinary wave, i.e. parallel to the Y axis. Then the diffracted wave is polarized as extraordinary one, i.e. its polarization vector belongs to the ZX plane and remains perpendicular to the wave vector of the diffracted wave. For each θ angle value, which we change from 0 to 180 deg with the steps 10–20 deg, the angle γ is changed by 360 deg (with the step 1 deg) in such a way that the wave vector of the diffracted wave rotates anticlockwise.

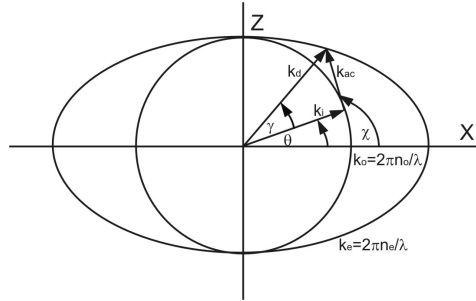


Fig. 1. Schematic vector diagram of anisotropic AO interaction in TeO_2 crystals.

As seen from Fig. 1, the direction of the AW vector changes when the angle θ does. For instance, we deal with a collinear AO diffraction whenever γ is equal to 0 or 180 deg. Then the three wave vectors, the wave vectors of the two optical waves and the AW, remain collinear. This kind of interaction cannot be accomplished when $\theta=90$ or 270 deg, since the birefringence is equal to zero along these directions. The direction of the AW vector is uniquely determined by the angle χ between the AW vector and the X axis:

$$\chi = \arctan \left(\frac{n_o n_e \frac{\sin(\theta + \gamma)}{\sqrt{n_o^2 \cos(\theta + \gamma) + n_e^2 \sin(\theta + \gamma)}} - n_o \sin \theta}{n_o n_e \frac{\cos(\theta + \gamma)}{\sqrt{n_o^2 \cos(\theta + \gamma) + n_e^2 \sin(\theta + \gamma)}} - n_o \cos \theta} \right). \quad (3)$$

The components of the strain tensor caused by the AW depend on the direction of the AW vector. So, we have a single nonzero strain tensor component e_1 for the longitudinal AW propagating along the X axis with the velocity $v_{11} = v_{QL}$. We deal with the only components e_5 or e_6 for the transverse waves polarized parallel to the Z axis ($v_{13} = v_{QT_1}$) or to the Y axis ($v_{12} = v_{QT_2}$). When the AW vector rotates by the angle χ , the strain tensor components for the longitudinal wave QL may be written as

$$e'_1 = e_1 \cos^2 \chi, \quad e'_3 = e_1 \sin^2 \chi, \quad e'_5 = e_1 \sin \chi \cos \chi. \quad (4)$$

We obtain similar relations for the transverse wave QT_1 ,

$$e'_1 = e_5 \sin 2\chi, \quad e'_3 = -e_5 \sin 2\chi, \quad e'_5 = e_5 \cos 2\chi, \quad (5)$$

and for the transverse wave QT_2 ,

$$e'_6 = 2e_6 \cos \chi, \quad e'_4 = -2e_6 \sin \chi. \quad (6)$$

If the anisotropic type of AO interactions occurs in the ZX plane, the electric field vector components for the diffracted wave are as follows:

$$E_1 = \Delta B_6 D_2, \quad E_3 = \Delta B_4 D_2, \quad (7)$$

$$E = \sqrt{E_1^2 + E_3^2}, \quad (8)$$

where D_2 is the electric displacement component for the incident wave, and ΔB_6 and ΔB_4 are the changes in optical-frequency impermeability tensor components occurring under the action of strains given by Eqs. (4)–(6). It is easily seen that no AO interaction is observed in the ZX plane for the AWs QL and QT₁, since all of the EOCs p_{61} , p_{63} , p_{65} , p_{41} , p_{43} and p_{45} are equal to zero for the symmetry group 422. Nonetheless, the AW QT₂ still can excite the AO interaction in the ZX plane. The corresponding impermeability increments become

$$\Delta B_6 = p_{66}e'_6 = 2p_{66}e_6 \cos \chi, \quad \Delta B_4 = p_{44}e'_4 = -2p_{44}e_6 \sin \chi. \quad (9)$$

Then Eq. (8) takes the form

$$E = 2e_6 D_2 \sqrt{p_{66}^2 \cos^2 \chi + p_{44}^2 \sin^2 \chi}, \quad (10)$$

and the EOC is defined by the relation

$$p_{ef} = 2\sqrt{p_{66}^2 \cos^2 \chi + p_{44}^2 \sin^2 \chi}. \quad (11)$$

After rotating the incident and diffracted optical wave vectors in the ZX plane we have to change the interaction plane by rotating it around the Z and X axes by the angles φ_Z and φ_X , respectively. The latter rotations modify the strains tensor components, which we write out for different AWs:

(i) for the QL wave

$$\begin{aligned} e''_1 &= e'_1 \cos^2 \varphi_Z, & e''_2 &= e'_1 \sin^2 \varphi_Z, \\ e''_3 &= e'_3, \\ e''_4 &= -e'_5 \sin \varphi_Z, & e''_5 &= e'_5 \cos \varphi_Z, & e''_6 &= -0.5e'_1 \sin \varphi_Z \cos \varphi_Z, \end{aligned}, \quad (12)$$

and

$$\begin{aligned} e'''_1 &= e'_1, & e'''_2 &= e'_3 \sin^2 \varphi_X, \\ e'''_3 &= e'_3 \cos^2 \varphi_X, \\ e'''_4 &= -0.5e'_3 \sin \varphi_X \cos \varphi_X, & e'''_5 &= e'_5 \cos \varphi_X, & e'''_6 &= -e'_5 \sin \varphi_X, \end{aligned} \quad (13)$$

where e'_1 , e'_3 and e'_5 are taken from Eqs. (4);

(ii) for the QT₁ wave

$$\begin{aligned} e''_1 &= e'_1 \cos^2 \varphi_Z, & e''_2 &= e'_1 \sin^2 \varphi_Z, \\ e''_3 &= e'_3, \\ e''_4 &= -e'_5 \sin \varphi_Z, & e''_5 &= e'_5 \cos \varphi_Z, & e''_6 &= -0.5e'_1 \sin \varphi_Z \cos \varphi_Z, \end{aligned}, \quad (14)$$

and

$$\begin{aligned} e'''_1 &= e'_1, & e'''_2 &= e'_3 \sin^2 \varphi_X, & e'''_3 &= e'_3 \cos^2 \varphi_X, \\ e'''_4 &= -0.5e'_3 \sin \varphi_X \cos \varphi_X, & e'''_5 &= e'_5 \cos \varphi_X, & e'''_6 &= -e'_5 \sin \varphi_X, \end{aligned} \quad (15)$$

where e'_1 , e'_3 and e'_5 are taken from Eqs. (5);

(iii) for the QT₂ wave

$$\begin{aligned} e''_1 &= e'_6 \sin \varphi_Z \cos \varphi_Z, \\ e''_2 &= -e'_6 \sin \varphi_Z \cos \varphi_Z, & e''_3 &= 0, \\ e''_4 &= e'_4 \cos \varphi_Z, & e''_5 &= e'_4 \sin \varphi_Z, & e''_6 &= e'_6 \cos 2\varphi_Z, \end{aligned} \quad (16)$$

and

$$\begin{aligned} e'''_1 &= 0, e'''_2 = -e'_4 \sin \varphi_X \cos \varphi_X, \\ e'''_3 &= e'_4 \sin \varphi_X \cos \varphi_X, \\ e'''_4 &= e'_4 \cos 2\varphi_X, e'''_5 = e'_6 \sin \varphi_X, e'''_6 = e'_6 \cos \varphi_X, \end{aligned} \quad (17)$$

where e'_4 and e'_6 are taken from Eqs. (6).

When the interaction plane is rotated around the Z and X axes, the electric displacement of the incident wave acquires the two components, D_1 and D_2 , while the electric field of the diffracted wave has all the three components, E_1 , E_2 and E_3 . Then Eqs. (7) have to be rewritten as $E_1 = \Delta B_1 D_1 + \Delta B_6 D_2$, $E_2 = \Delta B_6 D_1 + \Delta B_2 D_2$ and $E_3 = \Delta B_5 D_1 + \Delta B_4 D_2$ ($E = \sqrt{E_1^2 + E_2^2 + E_3^2}$). Substituting the impermeability tensor increments and the strain components given by Eqs. (12)–(17) into the mentioned formulae, one can derive the EOCs.

Note that two equivalent approaches can be used while determining the EOCs. The first has been elucidated in our work [1] as rewriting of the strain tensor in the new $X'Y'Z$ (or $XY'Z'$) coordinate system and, at the same time, leaving the EO tensor unchanged. The second approach, which is used here, lies in rewriting the EO tensor in the $X'Y'Z$ or $XY'Z'$ coordinate systems under the condition that the strain tensor is leaved unchanged. In other words, we will use Eqs. (4)–(6) for the strain tensor in the ZX plane, while the EO tensor will be rewritten based on the known relations $p''_{mnkl} = \alpha_{mr}(\varphi_Z) \alpha_{nt}(\varphi_Z) \alpha_{kp}(\varphi_Z) \alpha_{lq}(\varphi_Z) p_{rtpq}$ or $p'''_{mnkl} = \alpha_{mr}(\varphi_X) \alpha_{nt}(\varphi_X) \alpha_{kp}(\varphi_X) \alpha_{lq}(\varphi_X) p_{rtpq}$ (with ‘alpha’ matrices representing the rotational matrices). These formulae are concerned with the cases when the coordinate system is rotated respectively around the Z axis by the angle φ_Z or around the X axis by the angle φ_X .

The AOFM is defined as

$$M_2 = n_i^3 n_d^3 p_{ef}^2 / \rho v_{ij}^3, \quad (18)$$

where ρ is the density of optical material, $n_i = n_o$ the refractive index of the incident wave, $n_d = n_e^*$ the refractive index of the diffracted wave given by the relation

$$n_d = \left[\frac{n_o n_e}{\sqrt{(n_e^2 - n_o^2) \sin^2(\theta + \gamma) \cos^2 \varphi_x + n_0^2}} \right], \quad (19)$$

and v_{ij} denotes the AW velocity (with the indices i and j corresponding respectively to the AW propagation and polarization directions). One has to account for the dependence of AW velocities on the wave vector direction. The dependences of the quasi-transverse AW velocities on the wave vector orientation in the XZ plane are as follows:

$$\begin{aligned} v_{QT_1}^2(\chi) &= \frac{(C_{11} + C_{44}) \cos^2 \chi + \sin^2 \chi (C_{44} + C_{33})}{2\rho} - \\ &- \frac{\sqrt{[(C_{11} - C_{44}) \cos^2 \chi + (C_{44} - C_{33}) \sin^2 \chi]^2 + 4 \cos^2 \chi \sin^2 \chi (C_{13} + C_{44})^2}}{2\rho}, \end{aligned} \quad (20)$$

$$v_{QT_2}^2(\chi) = \frac{C_{44} \cos^2 \chi + C_{66} \sin^2 \chi}{\rho}. \quad (21)$$

The same relation for the quasi-longitudinal AW velocity takes the form

$$v_{QL}^2(\chi) = \frac{(C_{11} + C_{44})\cos^2 \chi + \sin^2 \chi(C_{44} + C_{33})}{2\rho} + \frac{\sqrt{[(C_{11} - C_{44})\cos^2 \chi + (C_{44} - C_{33})\sin^2 \chi]^2 + 4\cos^2 \chi \sin^2 \chi(C_{13} + C_{44})^2}}{2\rho}. \quad (22)$$

For the other interaction planes rotated by some angles φ_Z around the Z axis (i.e., in the new coordinate systems XYZ), the structure of the elastic stiffness tensor changes, too. The new tensor components can be determined after rewriting the tensor in this coordinate system according to a well-known procedure [8]. Performing this procedure for the elastic stiffness tensor, one can see that the components C'_{13} , $C'_{23} = C'_{13}$, C'_{33} and $C'_{44} = C'_{55}$ remain the same, whereas the dependences of the coefficients $C'_{11}(\varphi_Z)$, $C'_{22}(\varphi_Z) = C'_{11}(\varphi_Z)$, $C'_{12}(\varphi_Z)$ and $C'_{66}(\varphi_Z)$ on the angle φ_Z are described as

$$\left. \begin{aligned} C'_{11}(\varphi_Z) &= C_{11} - \frac{1}{2}(C_{11} - C_{12} - 2C_{66})\sin^2 2\varphi_Z \\ C'_{12}(\varphi_Z) &= C_{12} + \frac{1}{2}(C_{11} - C_{12} - 2C_{66})\sin^2 2\varphi_Z \\ C'_{66}(\varphi_Z) &= C_{66} + \frac{1}{2}(C_{11} - C_{12} - 2C_{66})\sin^2 2\varphi_Z \\ C'_{16}(\varphi_Z) &= -\frac{1}{4}(C_{11} - C_{12} - 2C_{66})\sin 4\varphi_Z \end{aligned} \right\}. \quad (23)$$

Notice that new elastic stiffness coefficients, $C'_{16} = -C'_{26}$, appear in the tensor thus rewritten.

It is worthwhile that the components of the Christoffel tensor for each of the XZ planes remain the same as for the initial XZ plane. Substituting Eq. (23) into Eqs. (20)–(22), one obtains the AW velocities for all of the possible AW vector directions. As seen from Eq. (23), the presence of four-fold axis among the symmetry operations of the crystal causes both optical and acoustic equivalences of a and b (or X and Y) axes. As a result, the crystallographic planes ac (XZ) and bc (YZ) are equivalent, too [8].

Rotation of the interaction plane by the angle φ_X around the X axis will change the Christoffel tensor components and the elastic stiffness coefficients C'_{13} , C'_{33} and C'_{44} . In particular, the Christoffel tensor becomes much more complicated. Then the AW velocities can be calculated using standard numeric techniques.

3. Results and discussion

One can obtain the formulae for the EOCs basing on the relations for the strain tensor components. For the interaction of type VII with the QL wave, the EOC is given by the relation

$$P_{ef}^{(VII)} = \sqrt{\left\{ \left[(p_{11}\cos^2 \varphi_Z + p_{12}\sin^2 \varphi_Z)\cos^2 \chi + p_{13}\sin^2 \chi \right] \cos \varphi_Z + p_{66}\cos^2 \chi \sin 2\varphi_Z \sin \varphi_Z \right\}^2 + \left\{ \left[(p_{21}\cos^2 \varphi_Z + p_{22}\sin^2 \varphi_Z)\cos^2 \chi + p_{23}\sin^2 \chi \right] \sin \varphi_Z + p_{66}\cos^2 \chi \sin 2\varphi_Z \cos \varphi_Z \right\}^2 + p_{44}^2 \sin^2 2\chi}, \quad (24)$$

when the interaction plane is rotated around the Z axis, and the relation

$$p_{ef}^{(VII)} = \sqrt{\left\{ p_{44} \sin 2\varphi_X \cos \varphi_X \sin^3 \chi + p_{55} \sin 2\chi \sin \chi \cos \varphi_X + \left(p_{31} \cos^2 \chi + p_{33} \sin^2 \chi \cos^2 \varphi_X \right) \sin \chi \sin \varphi_X \right\}^2 + \left\{ p_{44} \sin 2\varphi_X \sin \varphi_X \sin^3 \chi + p_{66} \sin 2\chi \sin \chi \sin \varphi_X + \left(p_{21} \cos^2 \chi + p_{23} \sin^2 \chi \cos^2 \varphi_X \right) \sin \chi \cos \varphi_X \right\}^2 + \left\{ p_{66} \sin 2\chi \sin \chi \sin \varphi_X \cos \varphi_X + p_{55} \sin 2\chi \sin \chi \sin \varphi_X \cos \varphi_X + \left(p_{11} \cos^2 \chi + p_{12} \sin^2 \chi \sin^2 \varphi_X + p_{13} \cos^2 \varphi_X \sin^2 \chi \right) \sin \chi \right\}^2}, \quad (25)$$

when the interaction plane is rotated around the X axis.

For the type VIII of the interaction with the QT₁ wave, we have the EOC

$$p_{ef}^{(VIII)} = \sqrt{\left\{ \left(p_{13} - p_{11} \cos^2 \varphi_Z - p_{12} \sin^2 \varphi_Z \right) \sin 2\chi \cos \varphi_Z + 0.5 p_{66} \sin 2\chi \sin 2\varphi_Z \sin \varphi_Z \right\}^2 + \left\{ \left(p_{23} - p_{21} \cos^2 \varphi_Z - p_{22} \sin^2 \varphi_Z \right) \sin 2\chi \sin \varphi_Z + 0.5 p_{66} \sin 2\chi \sin 2\varphi_Z \cos \varphi_Z \right\}^2 + p_{44}^2 \cos^2 2\chi \cos^2 2\varphi_Z}, \quad (26)$$

when the interaction plane is rotated around the Z axis, and

$$p_{ef}^{(VIII)} = \sqrt{\left\{ \left(p_{32} \sin^2 \varphi_X + p_{33} \cos^2 \varphi_X - p_{31} \right) \sin 2\chi \sin \chi \cos \varphi_X - 0.5 p_{44} \sin 2\chi \sin 2\varphi_X \sin \chi \cos \varphi_X + p_{55} \cos \varphi_X \cos 2\chi \sin \chi \right\}^2 + \left\{ \left(p_{22} \sin^2 \varphi_X + p_{23} \cos^2 \varphi_X - p_{21} \right) \sin 2\chi \sin \chi \cos \varphi_X - p_{66} \cos 2\chi \sin \chi \sin \varphi_X - 0.5 p_{44} \sin 2\chi \sin 2\varphi_X \sin \chi \sin \varphi_X \right\}^2 + \left\{ \left(p_{12} \sin^2 \varphi_X + p_{13} \cos^2 \varphi_X - p_{11} \right) \sin 2\chi \sin \chi - p_{66} \cos 2\chi \sin \chi \sin \varphi_X \cos \varphi_X + p_{55} \cos 2\chi \sin \chi \sin \varphi_X \cos \varphi_X \right\}^2}, \quad (27)$$

when the interaction plane is rotated around the X axis.

For the interaction of the type IX with the QT₂ wave we obtain the following EOCs:

$$p_{ef}^{(IX)} = \sqrt{\left\{ \left(p_{11} - p_{12} \right) \sin 2\varphi_Z \cos \varphi_Z \cos \chi + p_{66} \cos \chi \cos 2\varphi_Z \sin \varphi_Z \right\}^2 + \left\{ \left(p_{21} - p_{22} \right) \sin 2\varphi_Z \sin \varphi_Z \cos \chi + p_{66} \cos \chi \cos 2\varphi_Z \cos \varphi_Z \right\}^2 + p_{44}^2 \sin^2 \chi (\sin \varphi_Z + \cos \varphi_Z)^2}, \quad (28)$$

when the interaction plane is rotated around the Z axis, and

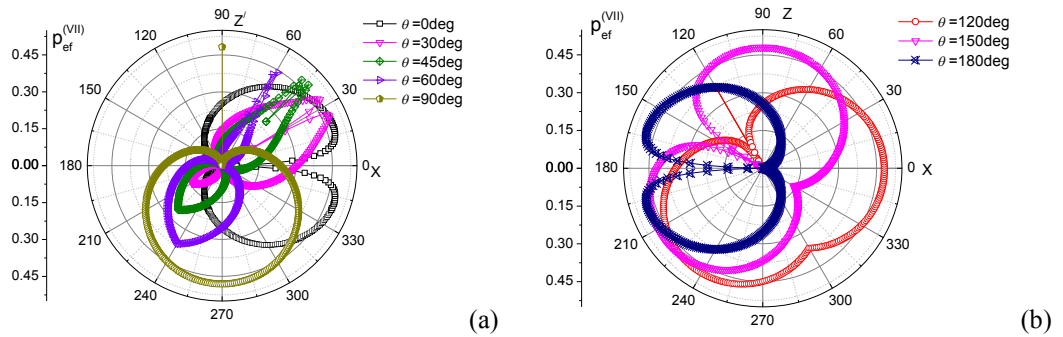
$$p_{ef}^{(IX)} = \sqrt{\left\{ \left(p_{32} - p_{33} \right) \sin 2\varphi_X \sin \varphi_X \sin^2 \chi + p_{44} \sin^2 \chi \cos 2\varphi_X \cos \varphi_X - 0.5 p_{55} \sin \varphi_X \sin 2\chi \right\}^2 + \left\{ \left(p_{22} - p_{23} \right) \sin 2\varphi_X \cos \varphi_X \sin^2 \chi + p_{44} \sin^2 \chi \cos 2\varphi_X \sin \varphi_X + 0.5 p_{66} \cos \varphi_X \sin 2\chi \right\}^2 + \left\{ \left(p_{12} - p_{13} \right) \sin 2\varphi_X \sin^2 \chi - p_{55} \sin 2\chi \sin^2 \varphi_X + 0.5 p_{66} \cos^2 \varphi_X \sin 2\chi \right\}^2}, \quad (29)$$

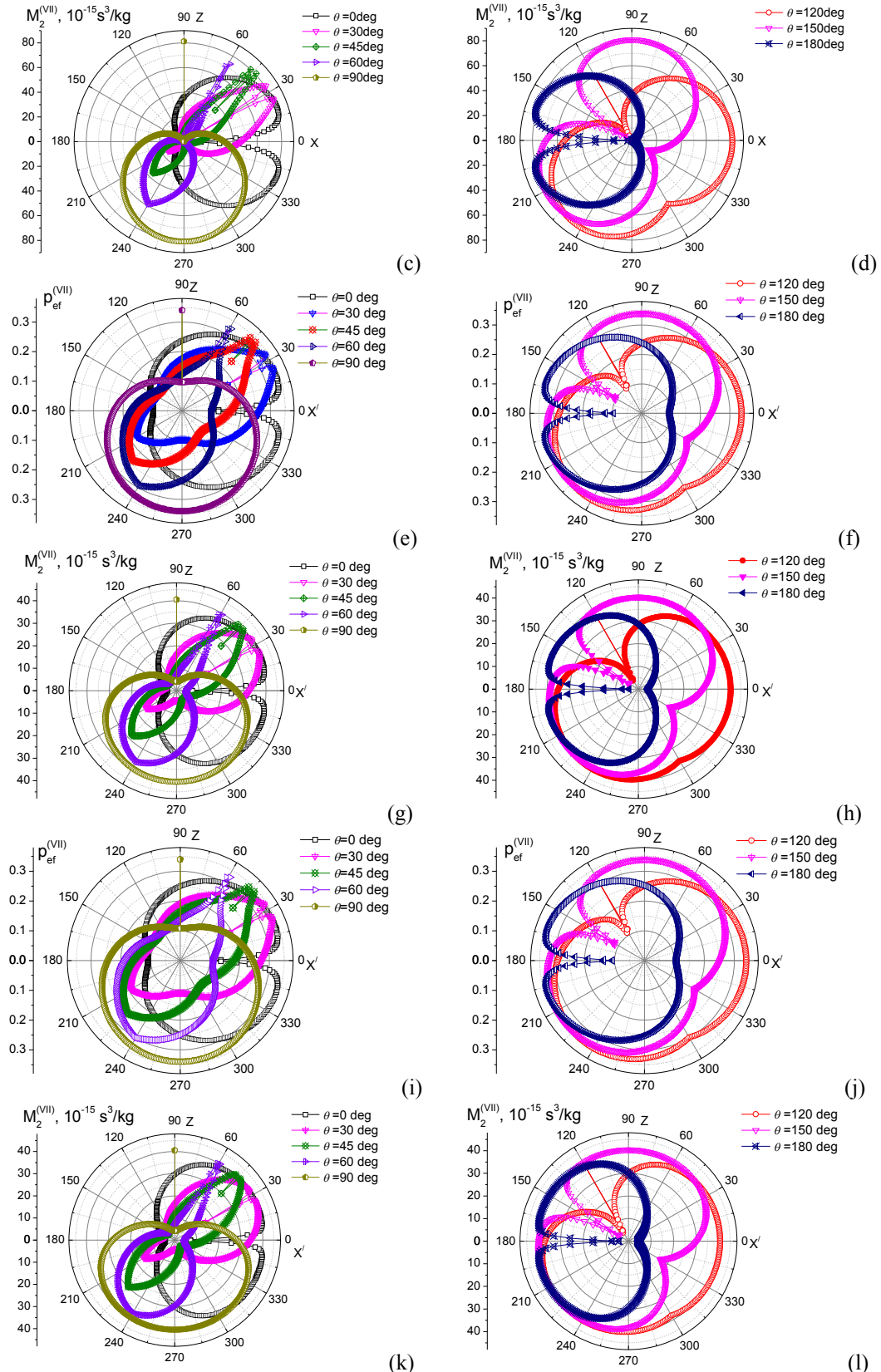
when the interaction plane is rotated around the X axis. Finally, to calculate the angular dependences of the AOEM, we have used the working formulae

$$\begin{aligned}
M_2^{(VII)} &= \frac{n_i^3 n_d^3 \left\{ p_{ef}^{(VII)} \right\}^2}{\rho [v_{QL}(\chi, \varphi_Z, \chi)]^3}, \\
M_2^{(VIII)} &= \frac{n_i^3 n_d^3 \left\{ p_{ef}^{(VIII)} \right\}^2}{\rho [v_{QT_i}(\chi, \varphi_Z, \chi)]^3}, \\
M_2^{(IX)} &= \frac{n_i^3 n_d^3 \left\{ p_{ef}^{(IX)} \right\}^2}{\rho [v_{QT_2}(\chi, \varphi_Z, \chi)]^3}.
\end{aligned} \tag{30}$$

Now we consider dependences of the EOC and the M_2 coefficient on the angle $\theta + \gamma$ at different angles of incidence θ and at different orientations of the interaction plane $X'Z$, which is defined by the angle φ_Z . Let us analyze the type VII of AO interactions that corresponds to the interaction with the longitudinal wave. As seen from Fig. 2, both the EOC and the AOFM reveal considerable anisotropy, which describe the AO interactions occurring in the ZX plane. The magnitude of the anisotropy depends on the angle of incidence θ and the sum of angles $\theta + \gamma$. It is interesting that the maximal EOC and AOFM are reached at the collinear diffraction when the wave vectors of the incident and diffracted waves are parallel. This phenomenon can be observed when the propagation directions of the two waves are close to the optic axis, i.e. the angle θ does not essentially differ from 90 deg. In this case the AOFM is equal to $\sim 40 \times 10^{-15} \text{ s}^3/\text{kg}$. The AOFM calculated for the case of collinear diffraction is characterized by a very sharp peak of the angular dependence. If we have $\theta = 0$ deg, the AOFM becomes minimal ($\sim 1.9 \times 10^{-15} \text{ s}^3/\text{kg}$). Then the angular dependence of the AOFM reveals a very sharp dip. The peaks and dips of the AOFM, which have already been observed for the collinear diffraction in the work [4], become almost indistinguishable when the interaction plane is rotated by $\varphi_Z = 90$ deg.

The maximal AOFM values for the case of non-collinear diffraction are reached at small diffraction angles when θ is close to 0 or 180 deg, as well as at the diffraction angles close to 180 deg (a so-called ‘reflection type’ of the diffraction), when the incidence angle θ is close to 90 deg. At $\varphi_Z = 90$ deg, the EOC and the AOFM are practically independent of either θ or $\theta + \gamma$ angles, thus being almost isotropic. The maximal AOFM that can be reached at the type VII of AO interactions in the plane ZX' does not exceed $\sim 42 \times 10^{-15} \text{ s}^3/\text{kg}$.





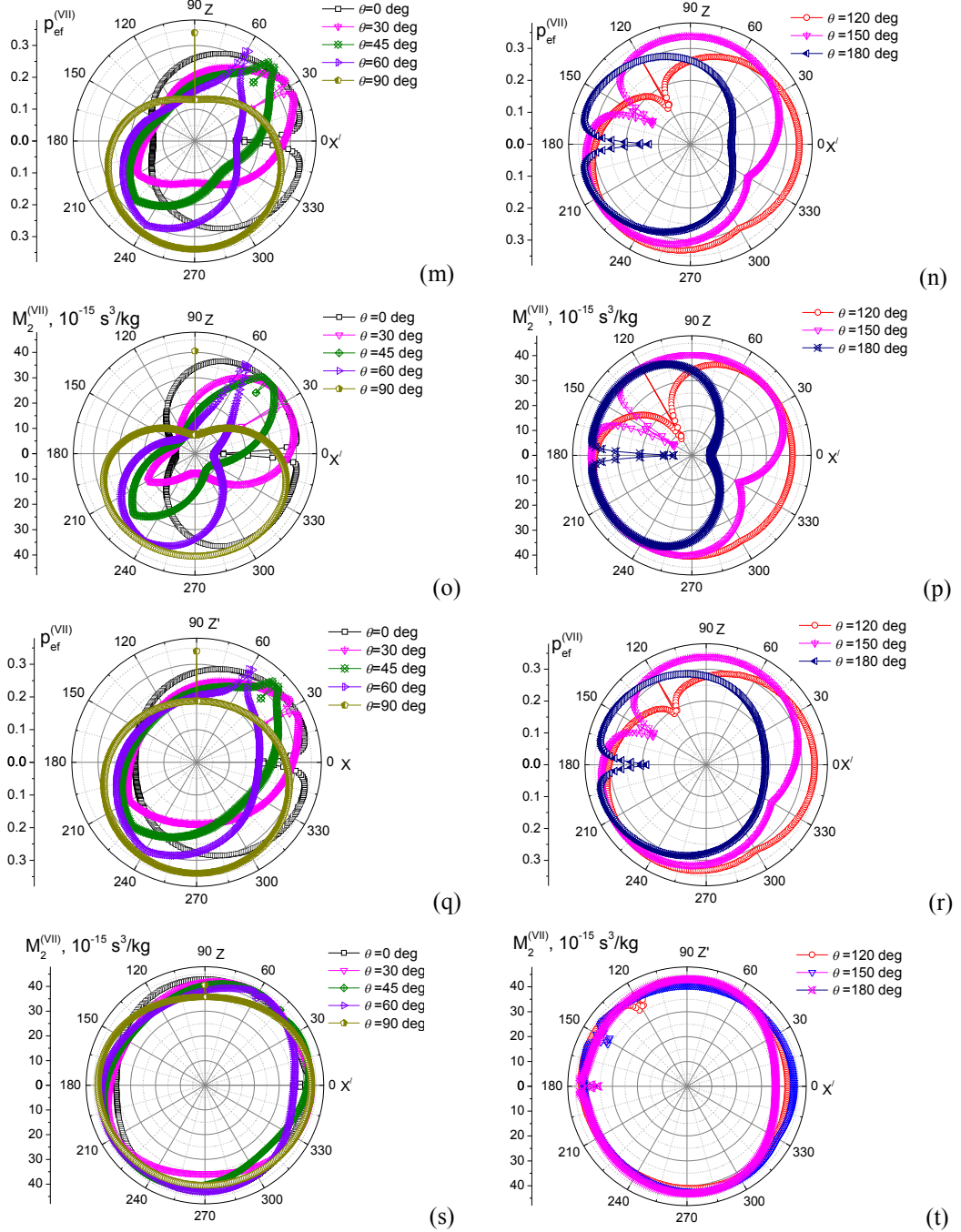
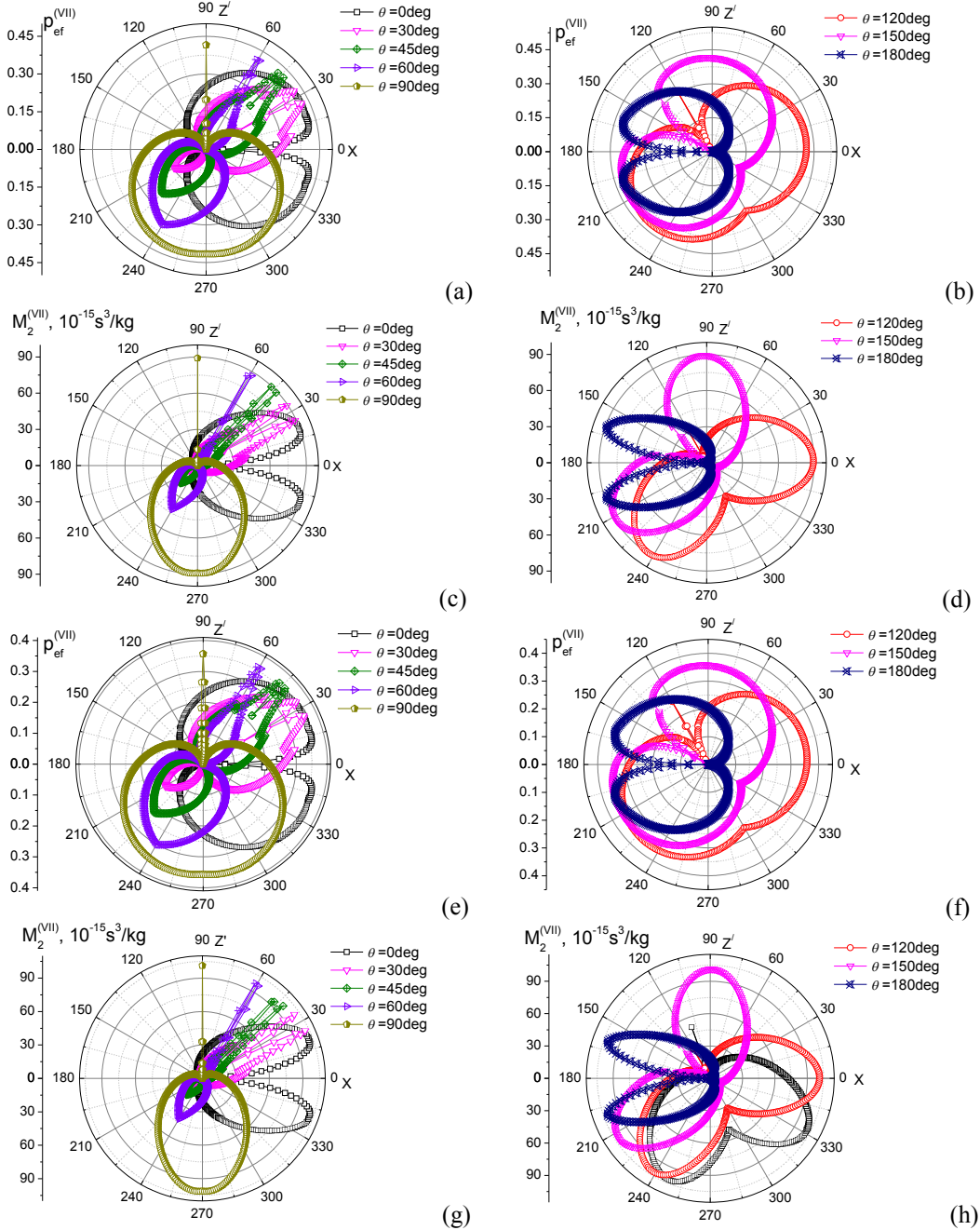


Fig. 2. Dependences of EOC (a, b, e, f, i, j, m, n, q, r) and AOFM (c, d, g, h, k, l, o, p, s, t) on the angle $\theta + \gamma$ at different incidence angles θ and for different orientations of the interaction plane $X'Z$ given by the angle φ_Z : $\varphi_Z = 0$ (a, b, c, d), 30 (e, f, g, h), 45 (i, j, k, l), 60 (m, n, o, p) and 90 deg (q, r, s, t). All the figures are associated with the type VII of AO interactions, i.e. the interaction with the longitudinal AW.

As seen from Fig. 3, the $M_2^{(VII)}$ maxima are reached in the range $30 \text{ deg} < \varphi_X < 60 \text{ deg}$. In particular, we have $101.5 \times 10^{-15} \text{ s}^3/\text{kg}$ at $\varphi_X = 45 \text{ deg}$. It turns out to be the highest maximum of AO FM for the type VII of AO interactions in TeO_2 crystals. At $\varphi_X = 90 \text{ deg}$ (in the interaction plane XY), one can observe an interesting peculiarity in the angular dependences of the EOC and the AO FM. Namely, if the angle θ is in the regions $\sim 10\text{--}50 \text{ deg}$ or $150\text{--}190 \text{ deg}$, abrupt changes in the EOC and the AO FM are observed at the diffraction angle $\gamma = \pm 20 \text{ deg}$. It is likely that these ‘jumps’ are caused by rapid angular changes of some of the terms appearing in the EOC, which result from pronounced nonlinearities of trigonometric functions.



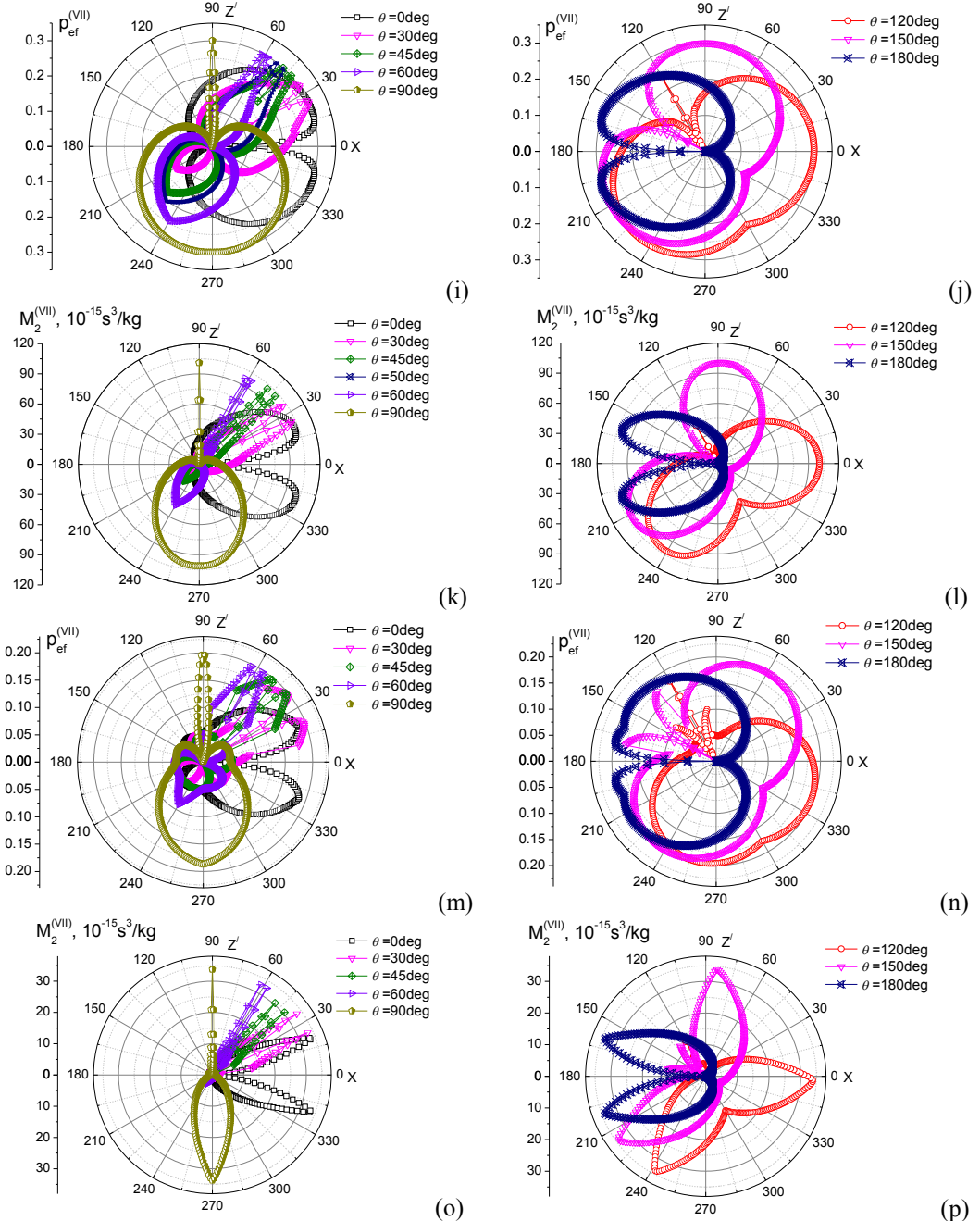
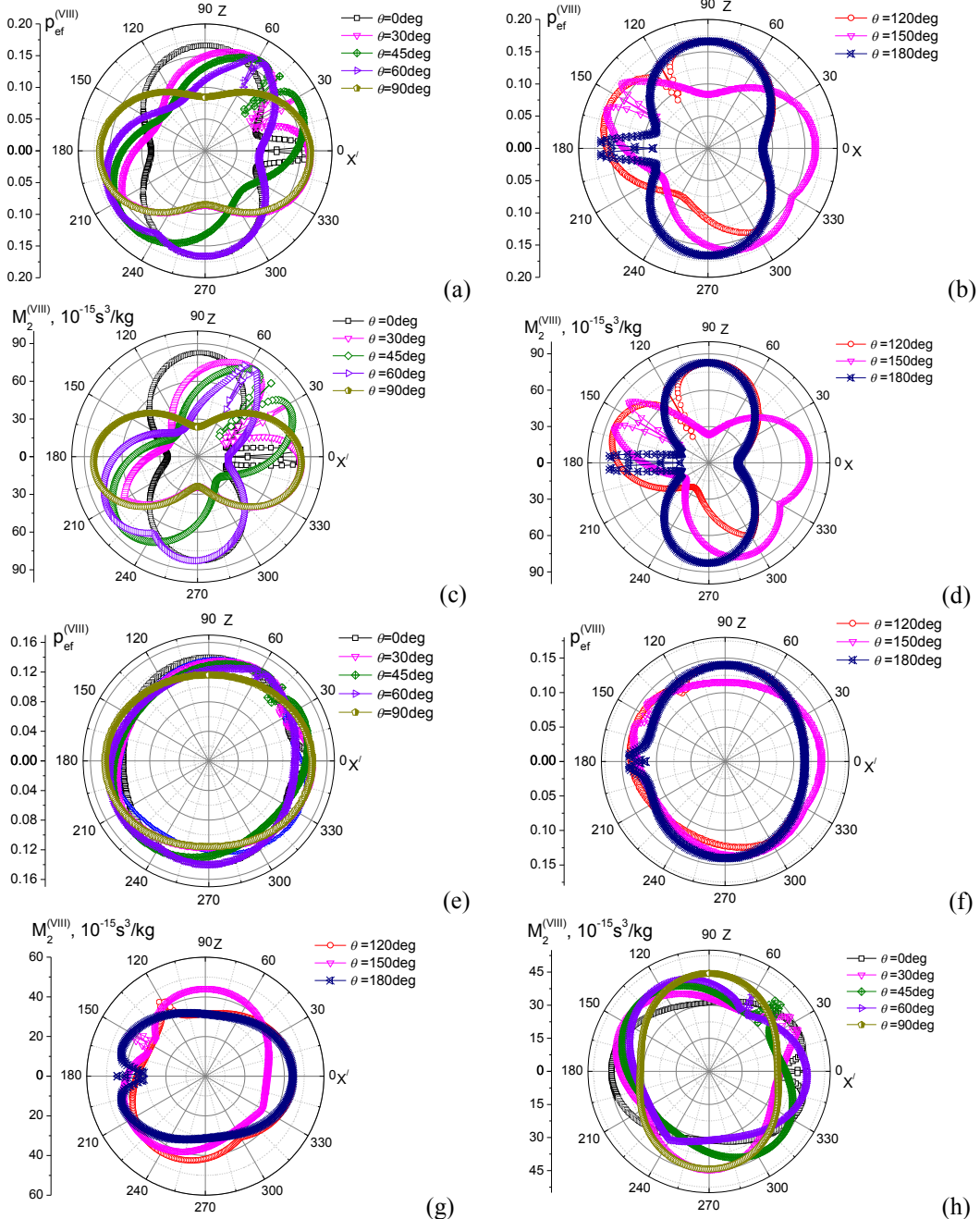
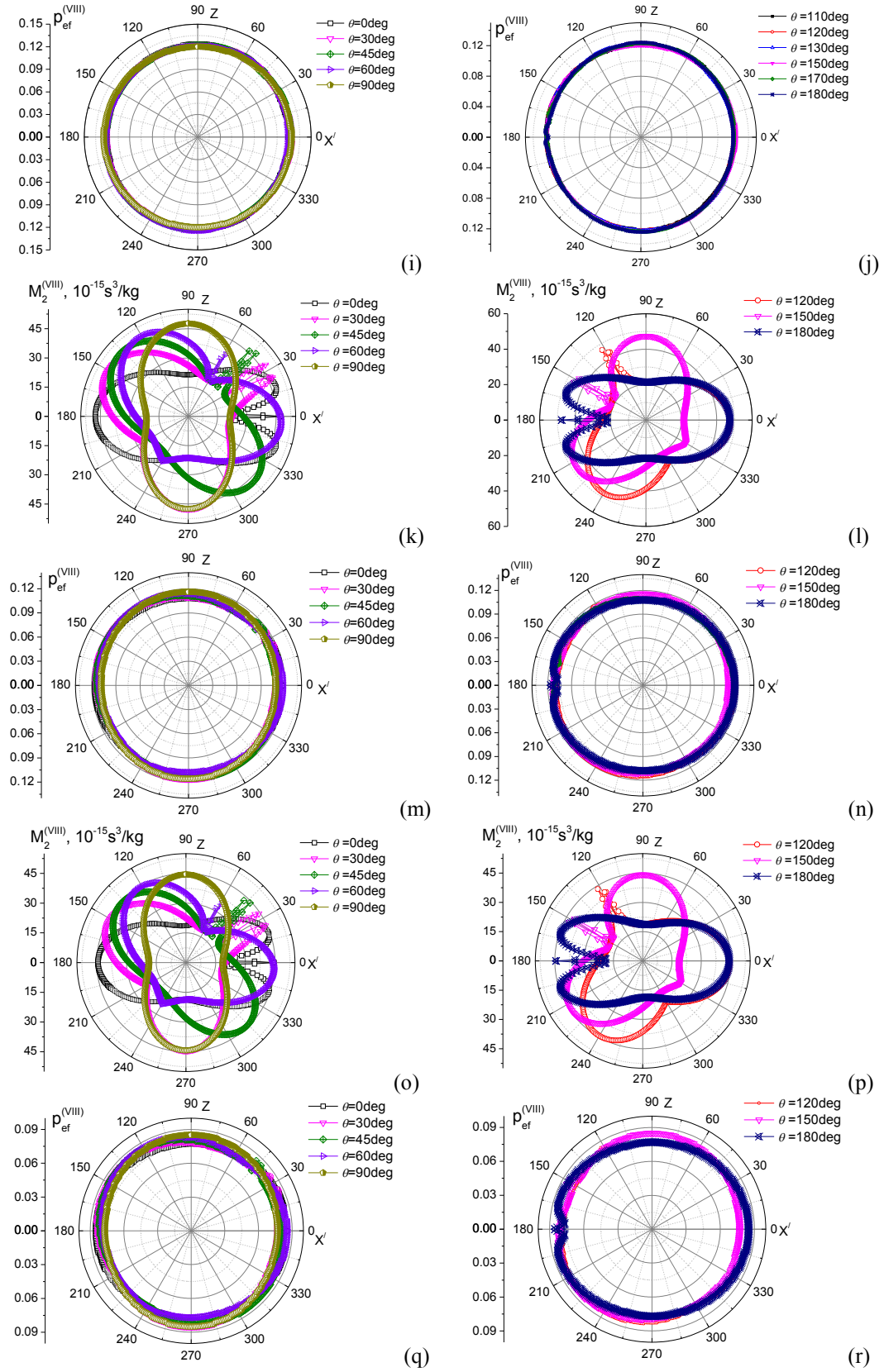


Fig. 3. Dependences of EOC (a, b, e, f, i, j, m, n) and AOFM (c, d, g, h, k, l, o, p) on the angle $\theta + \gamma$ at different incidence angles θ and for different orientations of the interaction plane XZ' given by the angle φ_X : $\varphi_X = 30$ (a, b, c, d), 45 (e, f, g, h), 60 (i, j, k, l) and 90 deg (m, n, o, p). All the figures are associated with the type VII of AO interactions, i.e. the interaction with the longitudinal AW.

If the type VIII of AO interactions in the plane $X'Z$ (Fig. 4) is dealt with, the maximal AOFM ($\sim 82 \times 10^{-15} \text{ s}^3/\text{kg}$) is reached when the interaction occurs in the ‘initial’ ZX plane. Due to rotation of the interaction plane around the Z axis, the AOFM decreases down to $24 \times 10^{-15} \text{ s}^3/\text{kg}$ (at $\varphi_Z = 90$ deg). Characteristics of the collinear diffraction are almost the same as those peculiar for the type VII of AO interactions. Notice that, although the EOC is almost isotropic at $\varphi_Z = 45, 60$ or 90 deg, the AOFM manifests a pronounced anisotropy, which must be caused by anisotropy of the corresponding AW slowness.





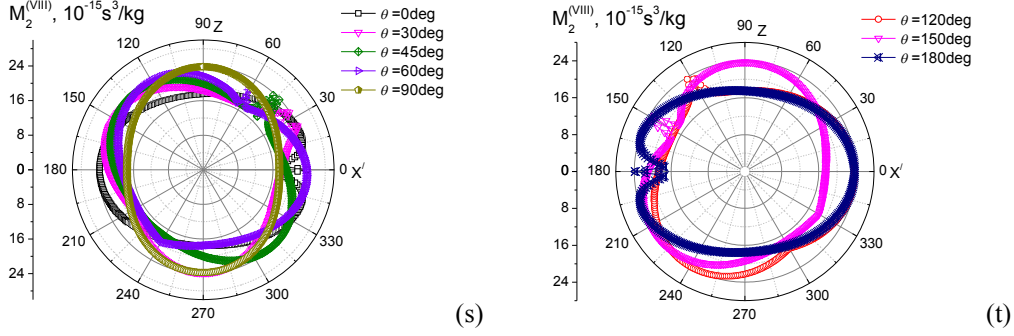
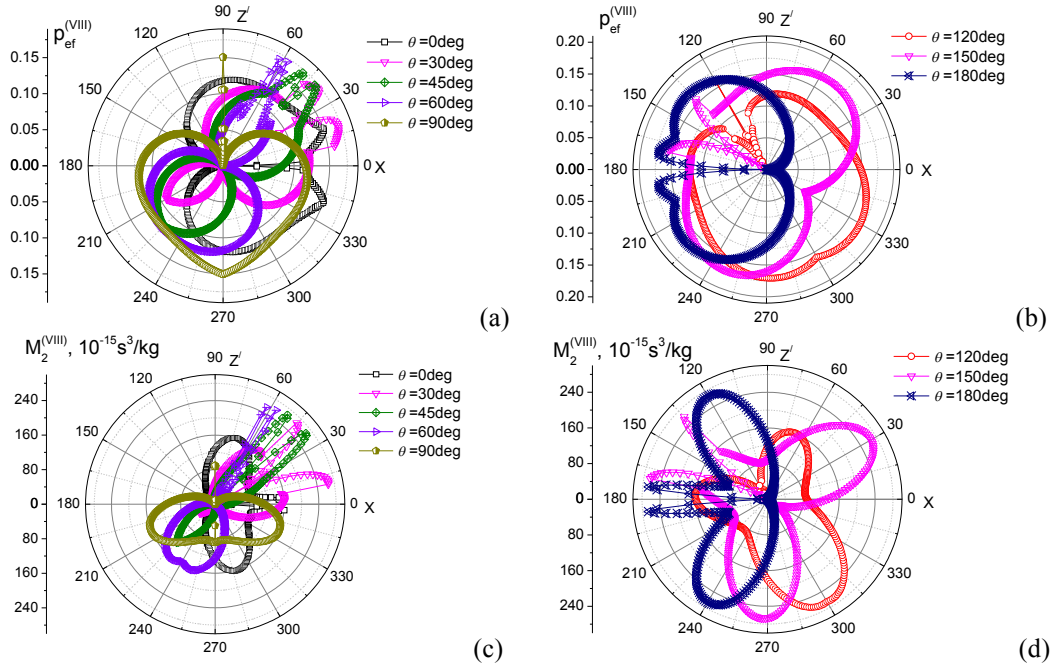
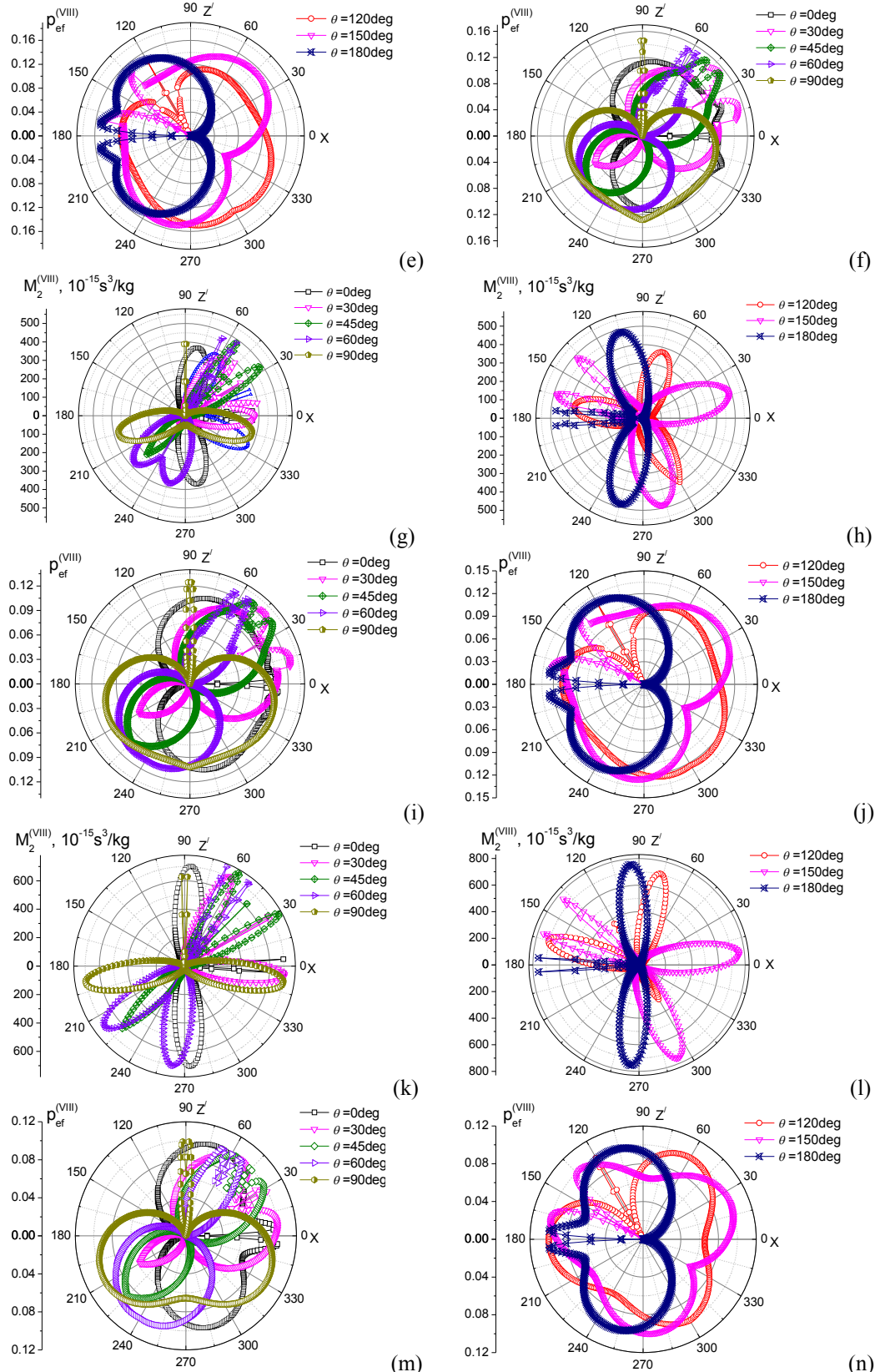


Fig. 4. Dependences of EOC (a, b, e, f, i, j, m, n, q, r) and AOFM (c, d, g, h, k, l, o, p, s, t) on the angle $\theta + \gamma$ at different incidence angles θ and for different orientations of the interaction plane $X'Z$ given by the angle φ_Z : $\varphi_Z = 0$ (a, b, c, d), 30 (e, f, g, h), 45 (i, j, k, l), 60 (m, n, o, p) and 90 deg (q, r, s, t). All the figures are associated with the type VIII of AO interactions, i.e. the interaction with the transverse AW $v_{13} = v_{Q\Gamma_1}$.

As seen from Fig. 5, the highest AOFM for the type VIII of AO interactions is reached at the diffraction in the XY plane, i.e. at $\varphi_X = 90$ deg. This value is equal to $929 \times 10^{-15} \text{ s}^3/\text{kg}$. So high M_2 is achieved because the AW velocity v_{13} is substituted with the velocity v_{12} whenever the interaction plane changes from XZ to XY . Notice that v_{12} is the slowest one and so the interaction with this wave results in drastic increase of the AOFM.





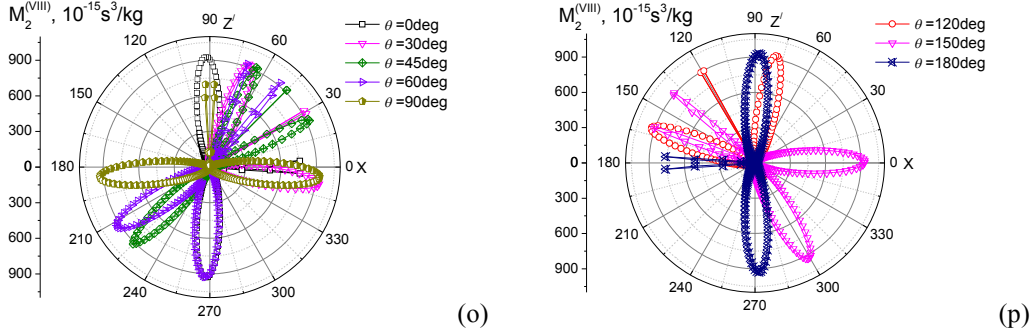
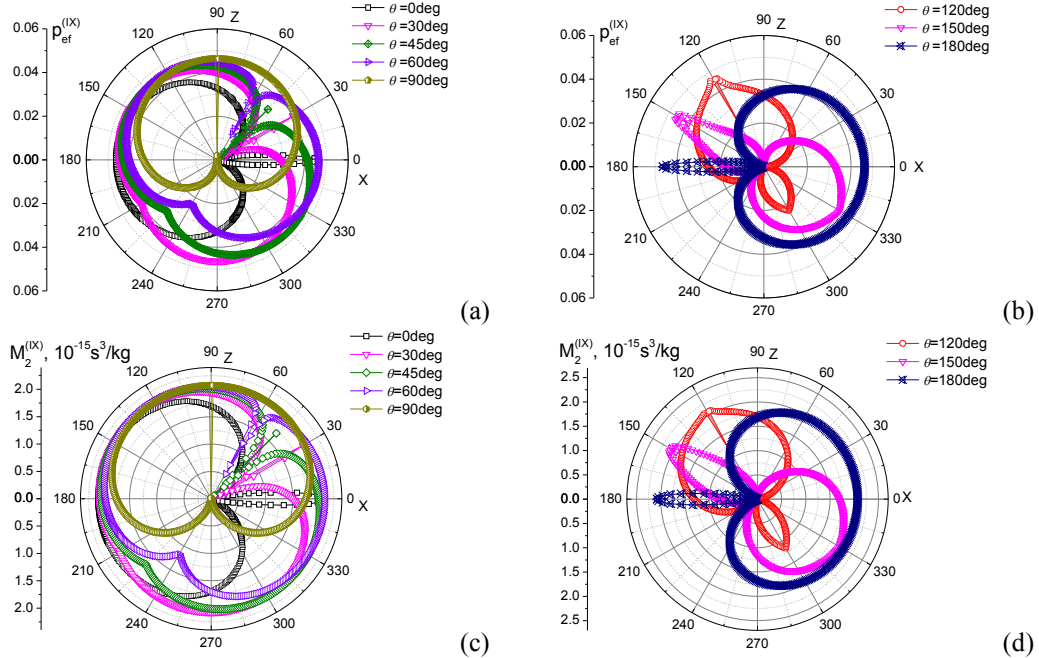
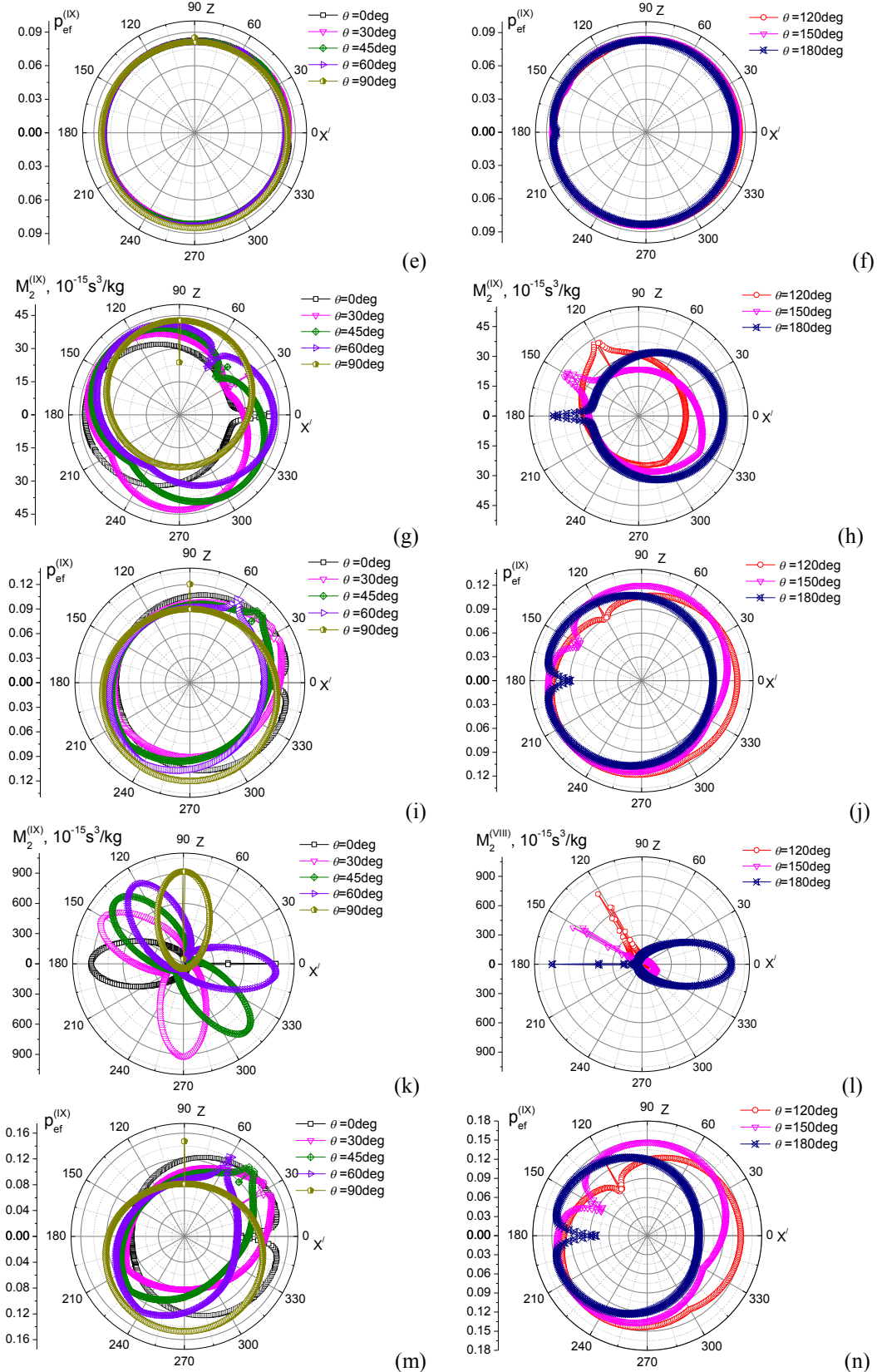


Fig. 5. Dependences of EOC (a, b, e, f, i, j, m, n) and AOFM (c, d, g, h, k, l, o, p) on the angle $\theta + \gamma$ at different incidence angles θ and for different orientations of the interaction plane XZ' given by the angle φ_X : $\varphi_X = 30$ (a, b, c, d), 45 (e, f, g, h), 60 (i, j, k, l) and 90 deg (m, n, o, p). All the figures are associated with the type VIII of AO interactions, i.e. the interaction with the transverse AW $v_{13} = v_{QT_1}$.

If the type IX of interactions with the transverse AW v_{12} is dealt with, the AOFM maximum ($\sim 916.5 \times 10^{-15} \text{ s}^3/\text{kg}$) is reached in the plane rotated by $\varphi_Z = 45$ deg. For the collinear AO interactions, this M_2 value is peculiar for the optical waves and the AWs propagating along the X' axis, i.e. along the bisector of the X and Y axes. For the non-collinear interactions, high M_2 values can be obtained, e.g., when the incident wave propagates along the optic axis (the Z axis, $\theta = 90$ deg) at small diffraction angles (e.g., at $\theta + \gamma \approx 85$ deg). In this case we obtain $M_2 = 900 \times 10^{-15} \text{ s}^3/\text{kg}$. This AOFM value can also be reached at any other incidence angles (see Fig. 6k, l).





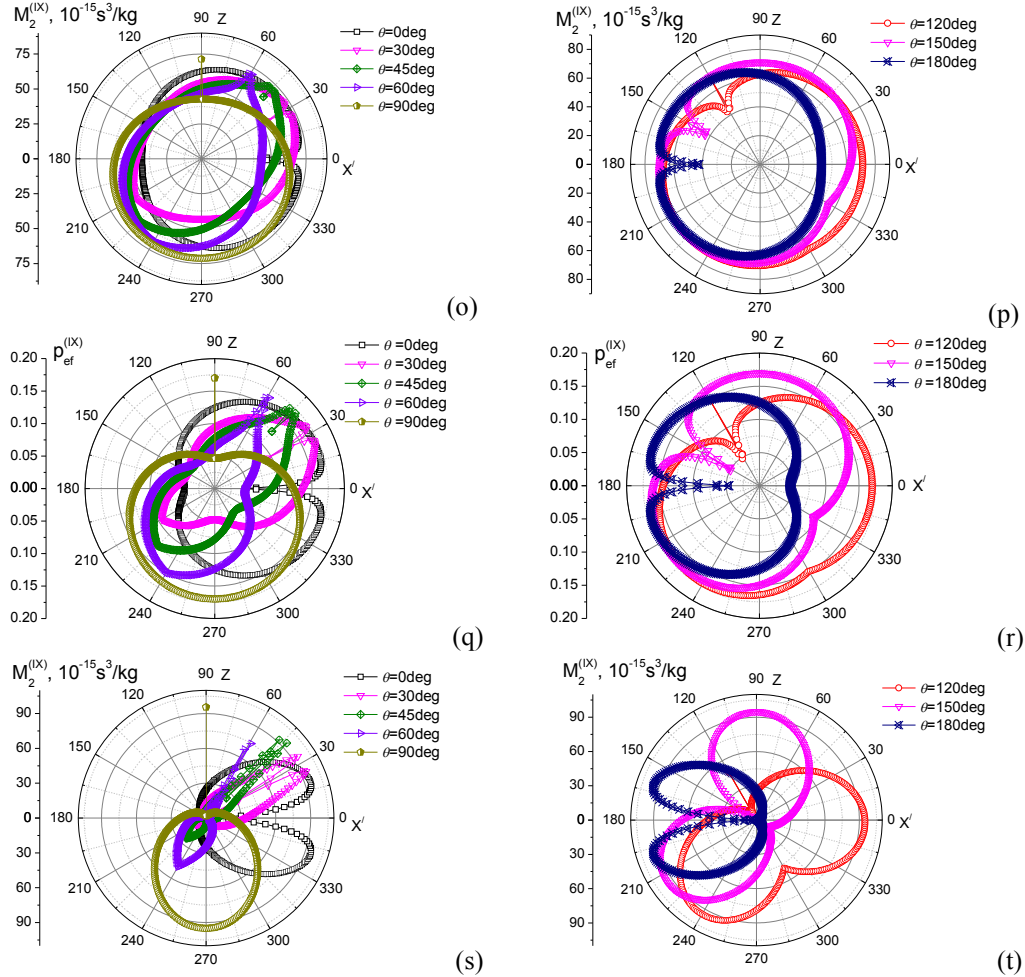
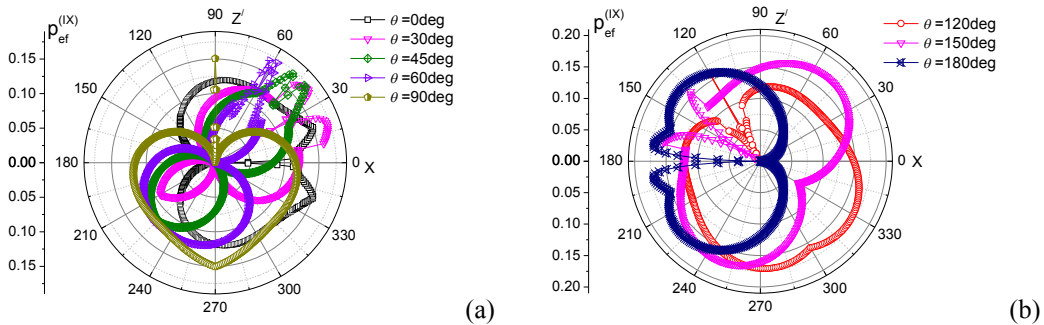
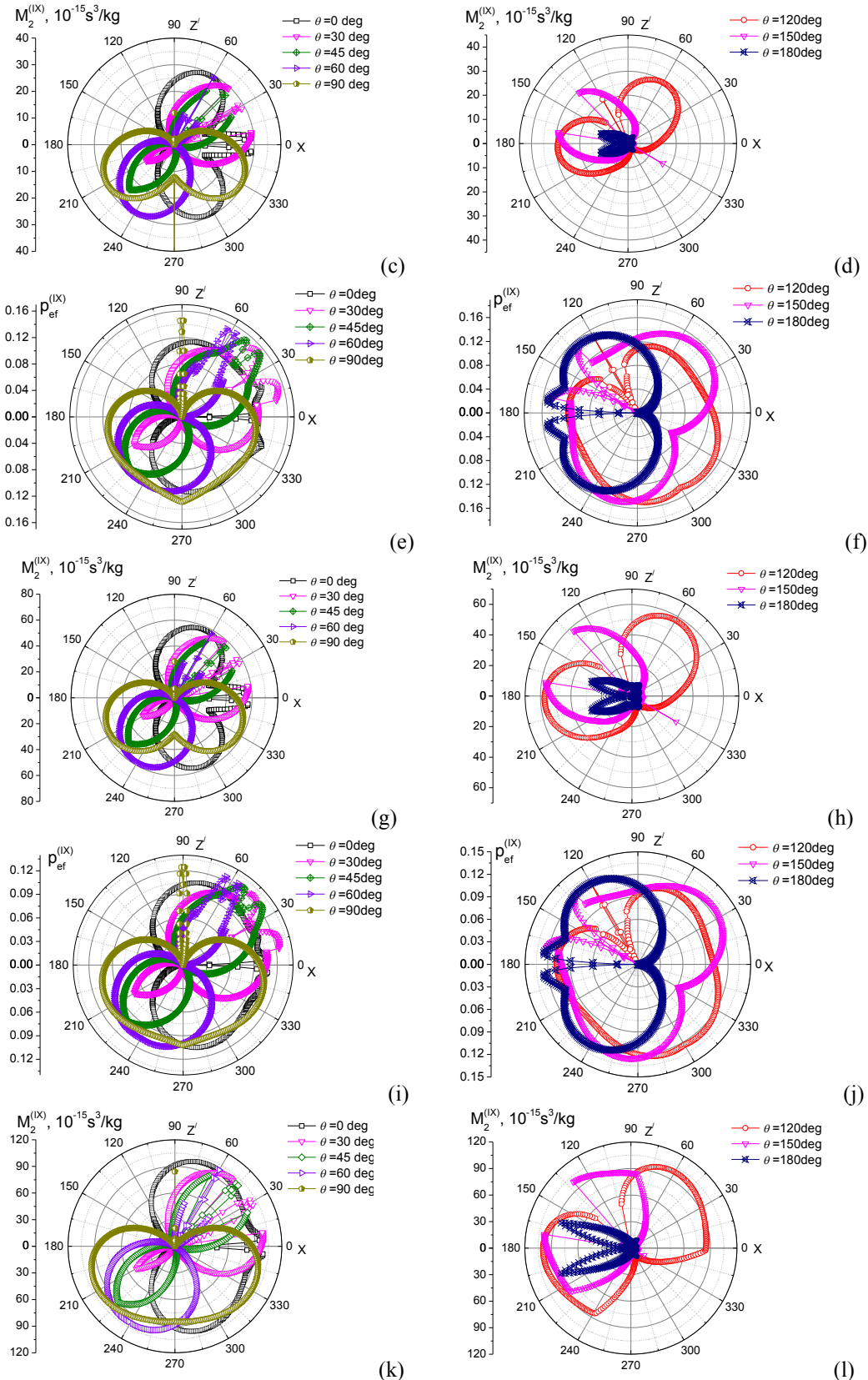


Fig. 6. Dependences of EOC (a, b, e, f, i, j, m, n, q, r) and AOFM (c, d, g, h, k, l, o, p, s, t) on the angle $\theta + \gamma$ at different incidence angles θ and for different orientations of the interaction plane $X'Z$ given by the angle φ_Z : $\varphi_Z = 0$ (a, b, c, d), 30 (e, f, g, h), 45 (i, j, k, l), 60 (m, n, o, p) and 90 deg (q, r, s, t). All the figures are associated with the type IX of AO interactions, i.e. the interaction with the transverse AW $v_{12} = v_{Q\Gamma_2}$.

As seen from Fig. 7 for the type IX of AO interactions, the AOFM increases with increasing φ_X angle. It reaches a maximum ($138 \times 10^{-15} \text{ s}^3/\text{kg}$) at $\varphi_X = 90$ deg (i.e., in the plane XY). Thus, the highest AOFM value for the type IX of AO interactions with the transverse wave v_{12} is peculiar for the interaction plane rotated by $\varphi_Z = 45$ deg. This value is equal to $\sim 916.5 \times 10^{-15} \text{ s}^3/\text{kg}$.





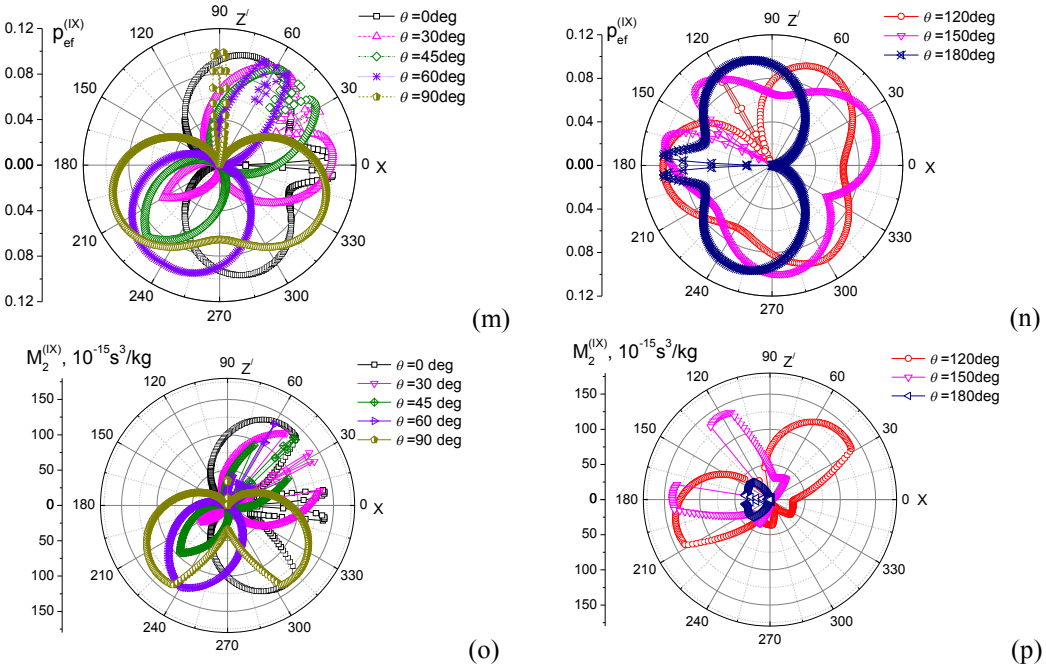


Fig. 7. Dependences of EOC (a, b, e, f, i, j, m, n) and AOFM (c, d, g, h, k, l, o, p) on the angle $\theta + \gamma$ at different incidence angles θ and for different orientations of the interaction plane XZ' given by the angle φ_X : $\varphi_X = 30$ (a, b, c, d), 45 (e, f, g, h), 60 (i, j, k, l) and 90 deg (m, n, o, p). All the figures are associated with the type IX of AO interactions, i.e. the interaction with the transverse AW $v_{12} = v_{QT_2}$.

Table 1 represents the AOFM values calculated for different types of anisotropic AO interactions in TeO_2 crystals, using the technique described above. One can see that the maximal AOFM is reached for the type VIII of AO interactions with the slowest transverse AW QT_1 , which propagates along the bisector of the X and Y axes and has polarization direction parallel to $[\bar{1}10]$. The AOFM for this case is equal to $929 \times 10^{-15} \text{ s}^3/\text{kg}$. As seen from figures presented above, the maximal AOFM values and, in particular, the highest one can be reached for different incidence angles of the optical wave. Then the angles of diffraction would differ, too. However, the parameters of the AW for which the AOFM maximum is achieved remain the same.

Now we will take into account all the results for the isotropic diffraction derived in the work [1] and the present analysis of the anisotropic diffraction in TeO_2 crystals for the optical waves of which polarization states correspond to the eigenstates. As a result, the highest AOFM value is peculiar for the isotropic interaction of the type III ($1143.8 \times 10^{-15} \text{ s}^3/\text{kg}$). It is achieved for the interaction with the same slow AW propagating with the velocity 612 m/s. The increasing in the AOFM from $929 \times 10^{-15} \text{ s}^3/\text{kg}$ (for the anisotropic diffraction) to $1143.8 \times 10^{-15} \text{ s}^3/\text{kg}$ (for the isotropic diffraction) is provided by moderate increases in the EOC and the refractive index.

Notice that the AOFM of TeO_2 crystals can still be slightly increased (up to $1200 \times 10^{-15} \text{ s}^3/\text{kg}$) if the incident optical wave is circularly polarized and propagates almost parallel to the optic axis [2]. However, the interaction conditions for the latter case are strongly limited by the requirements for the propagation directions of the incident and diffracted waves. Namely, these

waves have to propagate along the directions in which the eigenwaves are highly elliptic and a small linear birefringence exists. These conditions are satisfied whenever the both optical waves propagate close to the optic axis.

Table 1. Maximal values of the AOFM M_2 calculated for different types of anisotropic AO interactions in TeO_2 crystals, and description of the corresponding geometries.

Type of AO interaction	Angle $\varphi_{z,x}$ of orientation of the interaction plane	AW velocity, m/s	Type of AW	Directions of AW propagation and polarization	AOFM $M_2, 10^{-15} \text{ s}^3/\text{kg}$
VII	$\varphi_x = 45$ deg	3239	QL	[011], [011]	101.5
VIII	$\varphi_x = 90$ deg	612	QT ₁	[110], [$\bar{1}10$]	929.0
IX	$\varphi_z = 45$ deg	612	QT ₂	[110], [$\bar{1}10$]	916.5

Let us compare the efficiencies of the collinear AO diffractions in TeO_2 for different types of anisotropic interactions. As seen from Table 2, the AOFM maximum for the collinear AO interactions is achieved when the both optical waves and the slowest transverse AW propagate along the [110] direction. Then the AOFM equals to $916.5 \times 10^{-15} \text{ s}^3/\text{kg}$. Nonetheless, the AOFM for the collinear interaction with the longitudinal AW propagating along [011] is also high enough ($101.2 \times 10^{-15} \text{ s}^3/\text{kg}$).

Table 2. Maximal values of the AOFM M_2 calculated for different types of collinear anisotropic AO interactions in TeO_2 crystals, and description of the corresponding geometries.

Type of AO interaction	Angle $\varphi_{z,x}$ of orientation of the interaction plane	AW velocity, m/s	Type of AW	Direction of AW propagation and polarization	AOFM $M_2, 10^{-15} \text{ s}^3/\text{kg}$
VII	$\varphi_x = 45$ deg	3239	QL	[011], [011]	101.2
VIII	$\varphi_x = 90$ deg	612	QT ₁	[110], [$\bar{1}10$]	916.5
IX	$\varphi_z = 45$ deg	612	QT ₂	[110], [$\bar{1}10$]	916.5

4. Conclusions

Let us summarize the main results of the present study and our earlier work [1]. First, we have developed the approach for analyzing the anisotropy of AOFM for both the isotropic and anisotropic AO diffractions, and illustrated this approach on the example of TeO_2 crystals. We have shown that nine different types of AO interactions can be implemented in general. These are six types of the isotropic interactions and three types of the anisotropic interactions.

We have found out that the highest ($1143.8 \times 10^{-15} \text{ s}^3/\text{kg}$) AOFM value for TeO_2 crystals can be reached when the linearly polarized optical eigenwaves interact isotropically with the transverse AW QT₁. This AO diffraction belongs to the interaction type III. We have also demonstrated that the AOFM for the cases of collinear AO diffraction is characterized by sharp angular peaks or dips. The maximal AOFM value for the collinear diffraction is reached at the AO interactions of types VIII and IX with the AWs QT₁ and QT₂, respectively. These QT₁ and QT₂ waves should propagate along the direction [110] and be polarized along [$\bar{1}10$]. In the both cases, the AOFM is equal to $916.5 \times 10^{-15} \text{ s}^3/\text{kg}$. The maximal AOFM value for the anisotropic diffraction is equal to $929 \times 10^{-15} \text{ s}^3/\text{kg}$.

References

1. Mys O, Kostyrko M, Smyk M, Krupych O and Vlokh R, 2014. Anisotropy of acoustooptic figure of merit for TeO_2 crystals. 1. Isotropic diffraction. Ukr. J. Phys. Opt. **15**: 132–154.
2. Yano T and Watanabe A, 1974. Acousto-optic figure of merit of TeO_2 for circularly polarized light. J. Appl. Phys. **45**: 1243–1245.
3. Uchida N and Ohmachi Y, 1969. Elastic and photoelastic properties of TeO_2 single crystal. J. Appl. Phys. **40**: 4692–4695.
4. Zyuryukin Yu A, Zavarin S V and Yulaev A N, 2009. Characteristic features of wideband anisotropic light diffraction in lithium-niobate crystal by a longitudinal acoustic wave. Opt. Spectrosc. **107**: 152–156.
5. Yariv A and Yeh P. Optical waves in crystals. Propagation and control of laser radiation. New York: John Wiley & Sons (1984).
6. Shaskolskaya M P. Acoustic crystals. Moscow: Nauka (1982).
7. Uchida N, 1971. Optical properties of single-crystals paratellurite (TeO_2). Phys. Rev. B. **4**: 3736–3745.
8. Sirotin Yu I and Shaskolskaya M P. Fundamentals of crystal physics. Moscow: Nauka (1979).

Mys O., Kostyrko M., Krupych O. and Vlokh R. 2015. Anisotropy of acoustooptic figure of merit for TeO_2 crystals. 2. Anisotropic diffraction. Ukr.J.Phys.Opt. **16**: 38 – 60.

Анотація. У роботі представлена розроблений метод аналізу анізотропії коефіцієнта акустооптичної якості для анізотропної дифракції в оптично одновісних кристалах, а також проілюстровано його на прикладі кристалів парателуриту. Показано, що загалом реалізуються дев'ять типів акустооптичної взаємодії, шість з яких відповідають ізотропній дифракції, а три – анізотропній. Виявлено, що кутова залежність коефіцієнта акустооптичної якості для колінеарної дифракції характеризується гострими піком або впадиною. Максимальне значення коефіцієнта акустооптичної якості кристалів парателуриту при анізотропній дифракції досягається за умови акустооптичної взаємодії III-го типу з акустичною хвилею QT_1 , яка поширюється вздовж напрямку $[110]$ і поляризована вздовж $[\bar{1} \bar{1} 0]$. Коефіцієнт акустооптичної якості для цього типу дифракції дорівнює $929 \times 10^{-15} \text{ c}^3/\text{kg}$. Однак, найбільше значення коефіцієнта акустооптичної якості для кристалів парателуриту ($1143,8 \times 10^{-15} \text{ c}^3/\text{kg}$) досягається при ізотропній взаємодії власних лінійно поляризованих оптических хвиль із поперечною акустичною хвилею QT_1 (див. Mys O. et al., 2014. Ukr. J. Phys. Opt. **15**: 132). Ця акустооптична взаємодія відноситься до III-го типу. Результати наших розрахунків узгоджуються з літературними експериментальними даними.